Figures and figure supplements

Multiple 9-1-1 complexes promote homolog synapsis, DSB repair, and ATR signaling during mammalian meiosis

Catalina Pereira *et al*

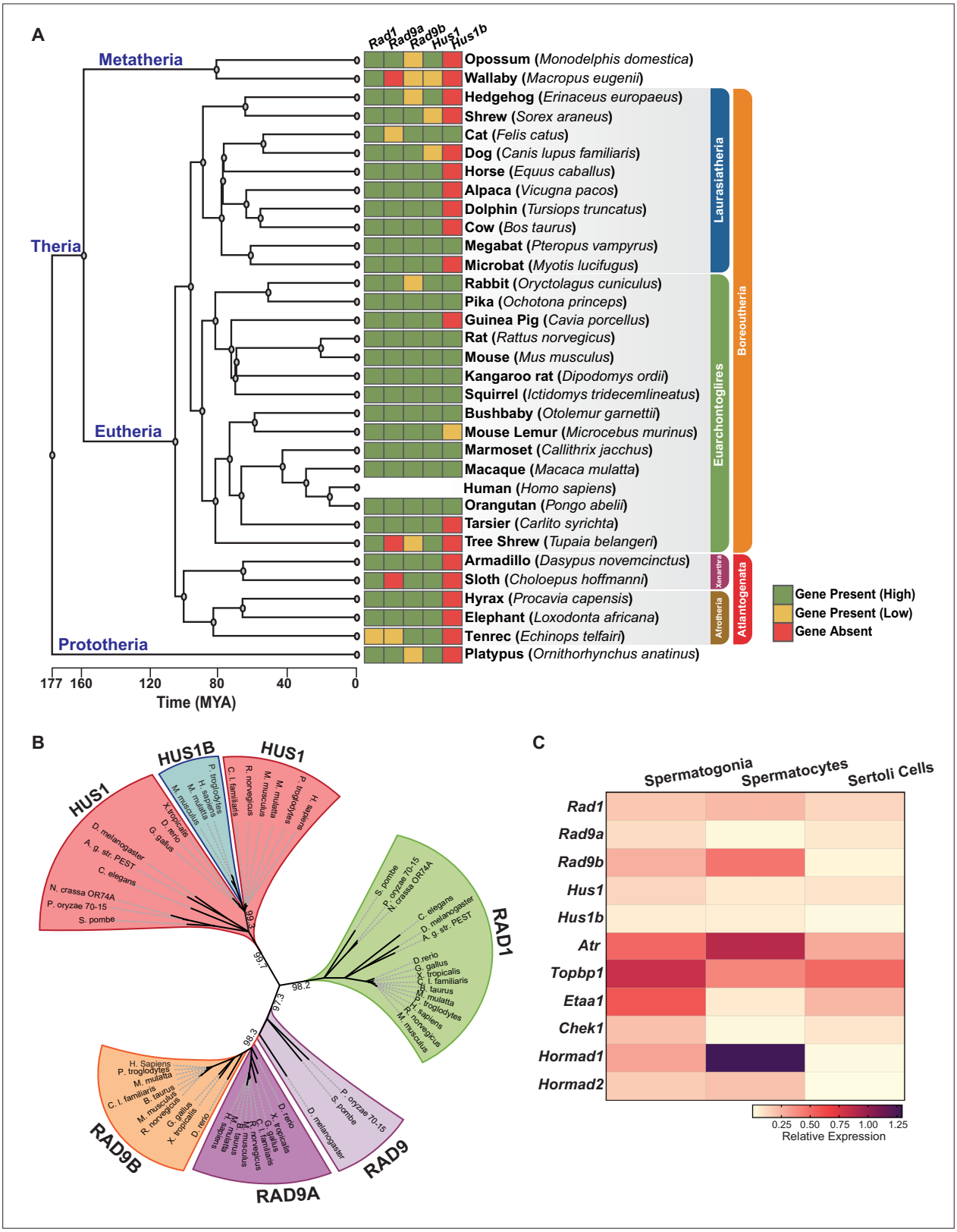

Figure 1. Phylogenetic analysis of 9-1-1 complex subunits. (**A**) Gene presence and absence matrix of human 9-1-1 subunit ortholog genes in 33 representative mammals. High confidence was determined if the genomic sequence had ≥50% of both target and query sequence identity, and a pairwise whole genomic alignment score of ≥50 when compared to human or if the genomic region containing the gene was syntenic with human. If an ortholog did not reach the threshold, then it was annotated as low confidence (yellow). If no ortholog was found, then it was considered absent

Figure 1 continued on next page

Figure 1 continued

(red). A cladogram was obtained from timetree.org. (**B**) Maximum likelihood unrooted phylogenetic tree of 9-1-1 subunit genes based on JTT + I + G + F. Protein sequences were obtained from NCBI HomoloGene and include bacteria (*Pleomorphomonas oryzae*), fungi (*Schizosaccharomyces pombe, Neurospora crassa*), nematode (*Caenorhabditis elegans),* true flies (*Drosophila melanogaster, Anopheles gambiae* str. *Pest*), fish (*Danio rerio*), frog (*Xenopus tropicalis*), bird (*Gallus gallus*), carnivora (*Canis lupus*), rodents (*Rattus norvegicus, Mus musculus*), and primates (*Homo sapiens, Mus musculus, Macaca mulatta, Pan troglodytes*). Sequences were aligned by Clustal Omega, and substitution model was tested on ProtTest. Ultrafast bootstrap (×1000 replicates) was performed in IQ-TREE web server, and nodes below 70% branch support were collapsed. Branch distance represents substitution rate. The lighter purple RAD9 denotes RAD9 prior to the duplication event. (**C**) Heatmap of single-cell RNA-sequencing data from mouse testes was queried to assess the expression of the indicated genes in spermatogonia, spermatocytes, and Sertoli cells. Expression of *Rad9b* in spermatocytes, p-value ≤ $5.47e^{-10}$, *Rad1* p-value ≤ $1.20e^{-09}$, *Hus1b* p-value ≤ $1.08e^{-08}$. Expression of *Rad9a* and *Hus1* in spermatogonia p-value ≤ $5.61e^{-19}$; p-value ≤ $3.78e^{-09}$. Relative expression is shown for each gene, with highest expression observed in purple and lowest expression observed in yellow.

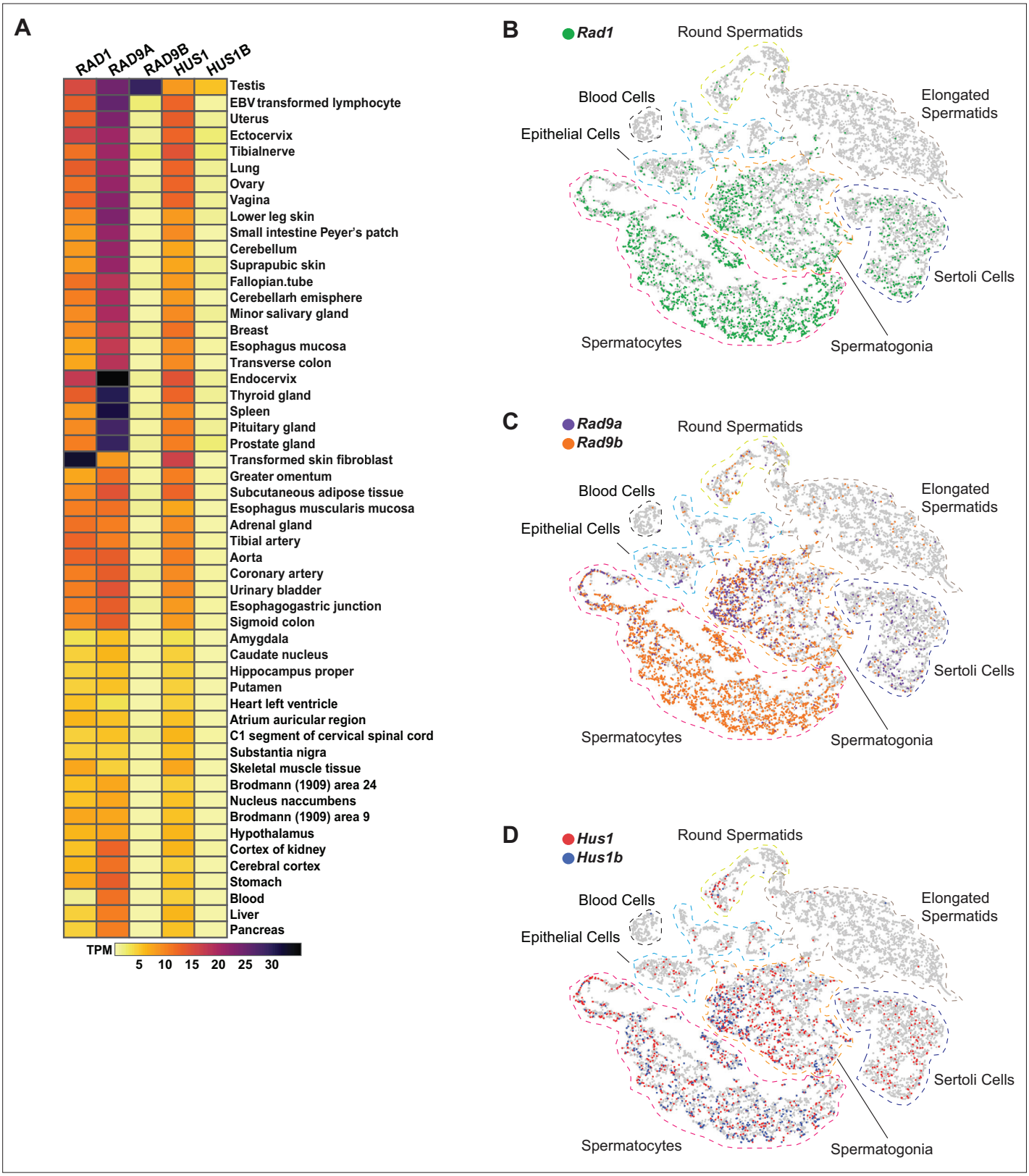

Figure 1—figure supplement 1. Expression of 9-1-1 complex subunits. (**A**) Expression of 9-1-1 subunits in various human tissues. Data from the Genotype-Tissue Expression (GTEx) project was obtained in Expression Atlas – EMBL-EBI. Gene expression values are shown as transcript per million (TPM). (**B–D**) tSNE plots of single-cell RNA-seq analysis of mouse testes demonstrating the expression of 9-1-1 subunits in single cells from round spermatids, elongated spermatids, blood cells, epithelial, spermatocytes, spermatogonia, and Sertoli cells population within testes. Gray circles are

Figure 1—figure supplement 1 continued on next page

Figure 1—figure supplement 1 continued

individual cells. (**B**) *Rad1*-expressing cells are shown in green. (**C**) *Rad9a*-expressing cells are shown in purple, and *Rad9b*-expressing cells are in orange. (**D**) *Hus1*-expressing cells are in red, and *Hus1b*-expressing cells are in blue.

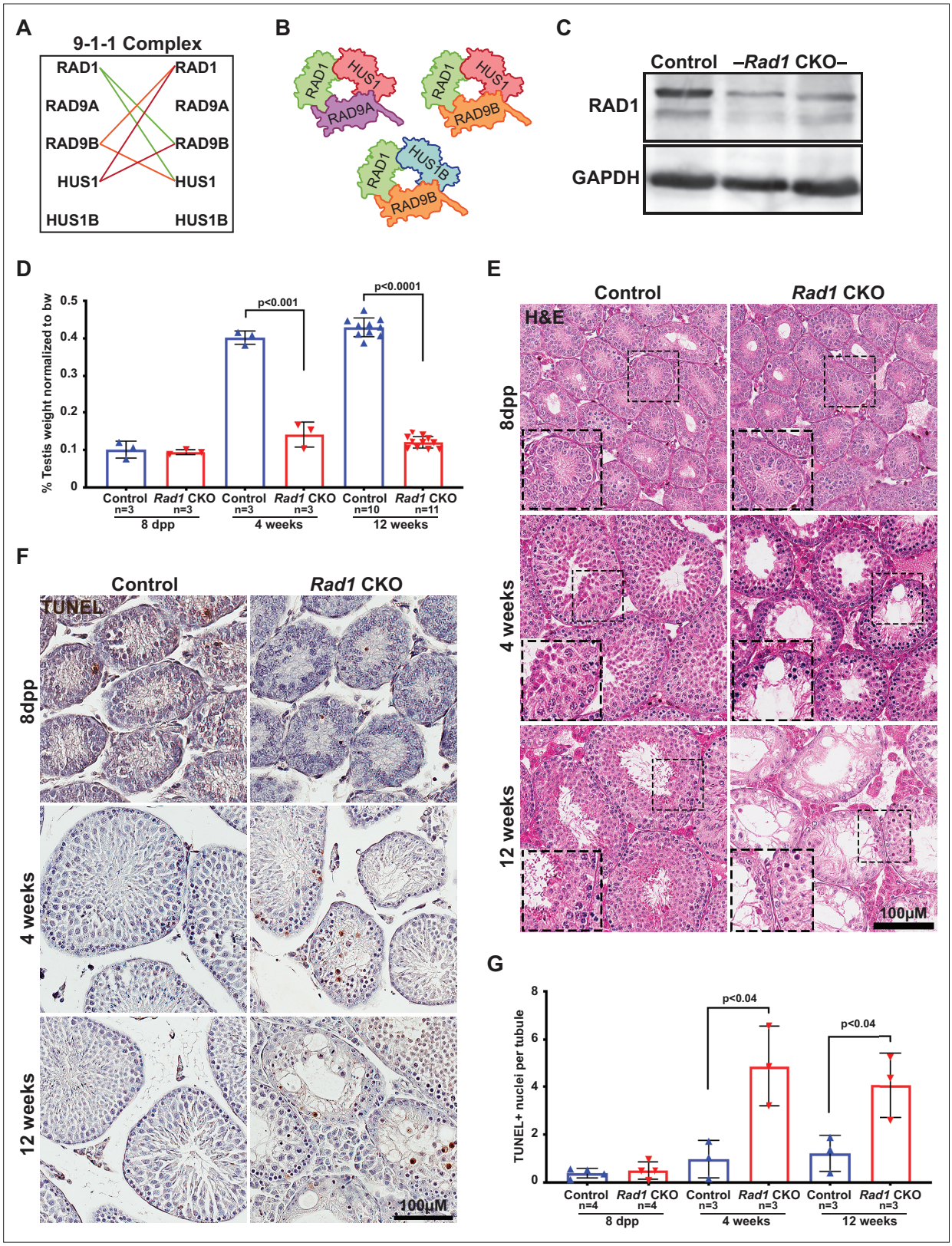

Figure 2. Conditional knockout (CKO) of the 9-1-1 complex subunit RAD1 causes severe germ cell loss in testes. (**A**) Evolutionary rate covariation analysis between 9-1-1 subunits. Lines depict significant covariance between 9-1-1 subunits. (**B**) Schematic showing putative meiotic 9-1-1 complexes: 9A-1-1, 9B-1-1, and 9B-1-1B. (**C**) Representative immunoblot for RAD1 in control and *Rad1* CKO whole testes lysates from 12-week-old mice (n = 5 control and 5 CKO samples analyzed in total). (**D**) Testis weight normalized to body weight from 8-day postpartum (dpp), 4-week-old, and 12-week-

Figure 2 continued on next page

Figure 2 continued

old control and *Rad1* CKO mice. (**E**) Seminiferous tubule cross sections from 8-dpp, 4-week-old, and 12-week-old mice were stained with H&E (representative images from three mice analyzed per age group per genotype). (**F, G**) Representative images (**F**) and quantification (**G**) of TUNEL-positive cells per tubule in control and *Rad1* CKO mice (50 tubules per mouse quantified; n = number of mice analyzed). p-Value calculated using Welch's unpaired *t*-test in GraphPad.

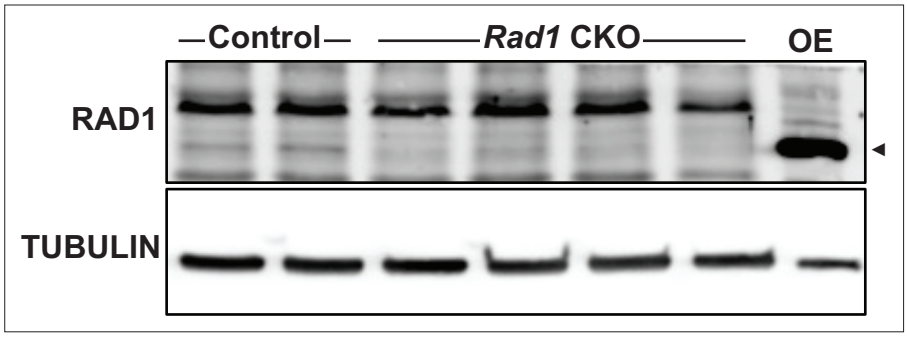

Figure 2—figure supplement 1. RAD1 levels are reduced in juvenile testes. Immunoblotting for RAD1 in control (n = 2) and *Rad1* conditional knockout (CKO) (n = 4) whole testes lysates from 14-day-old mice. The last lane contains cell lysate from 293T cells transiently overexpressing (OE) mouse RAD1. Arrowhead marks the location of the RAD1 band.

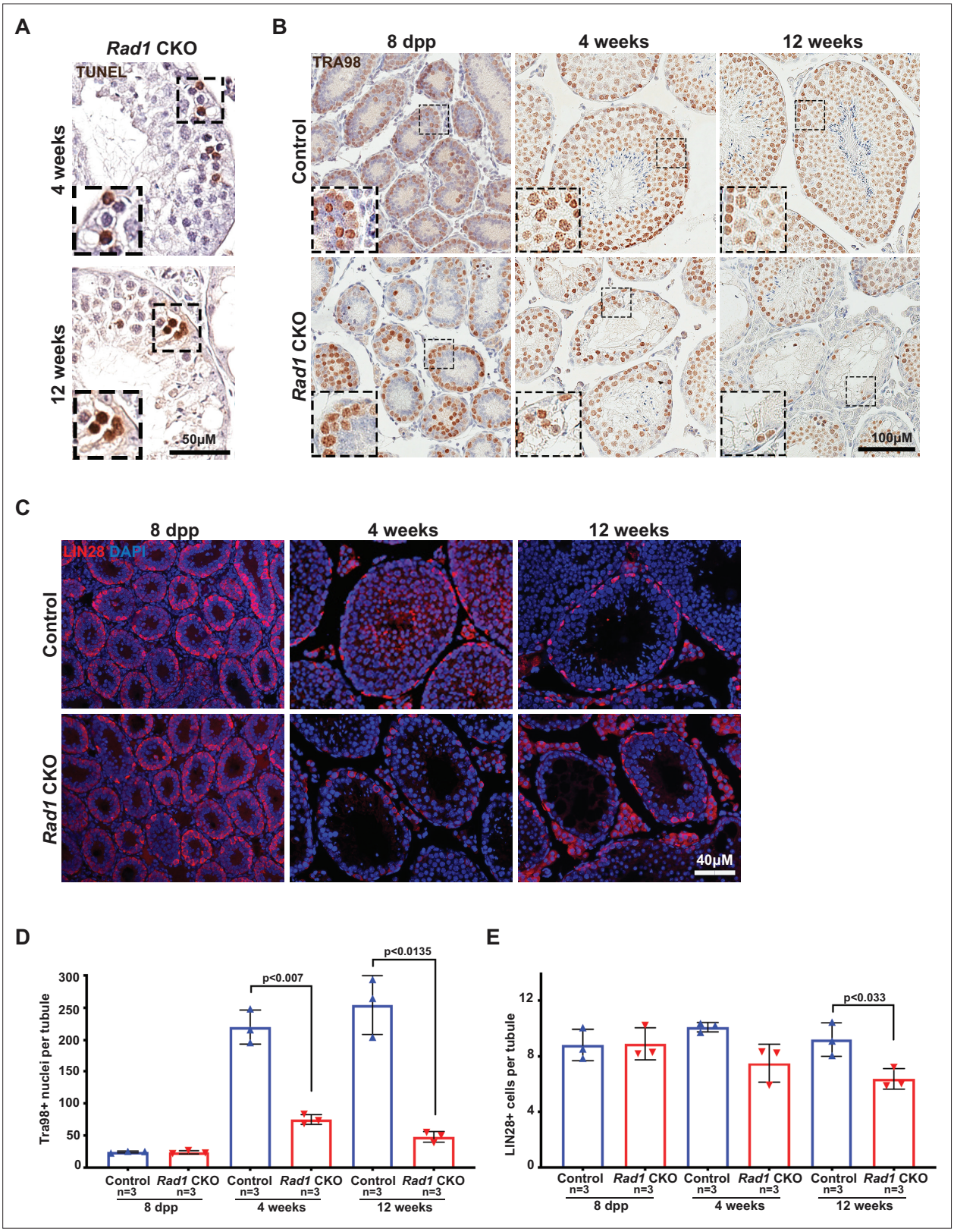

Figure 2—figure supplement 2. *Rad1* inactivation in testis causes germ cell loss. (**A**) Representative images of zygotene/pachytene-stage TUNEL-positive cells from 4 week-old and 12 week-old *Rad1* conditional knockout (CKO) testes. (**B, C**) Representative images of TRA98-positive cells (**B**) and LIN-28-positive spermatogonial stem cells (**C**) in testis sections from control and *Rad1* CKO mice. (**D**) Quantification of TRA98-positive cells (n = number of mice; 50 tubules per mouse quantified). (**E**) Quantification of LIN28-positive spermatogonial stem cells (n = number of mice; 50 tubules per mouse quantified). p-Value calculated using Welch's unpaired *t*-test in GraphPad.

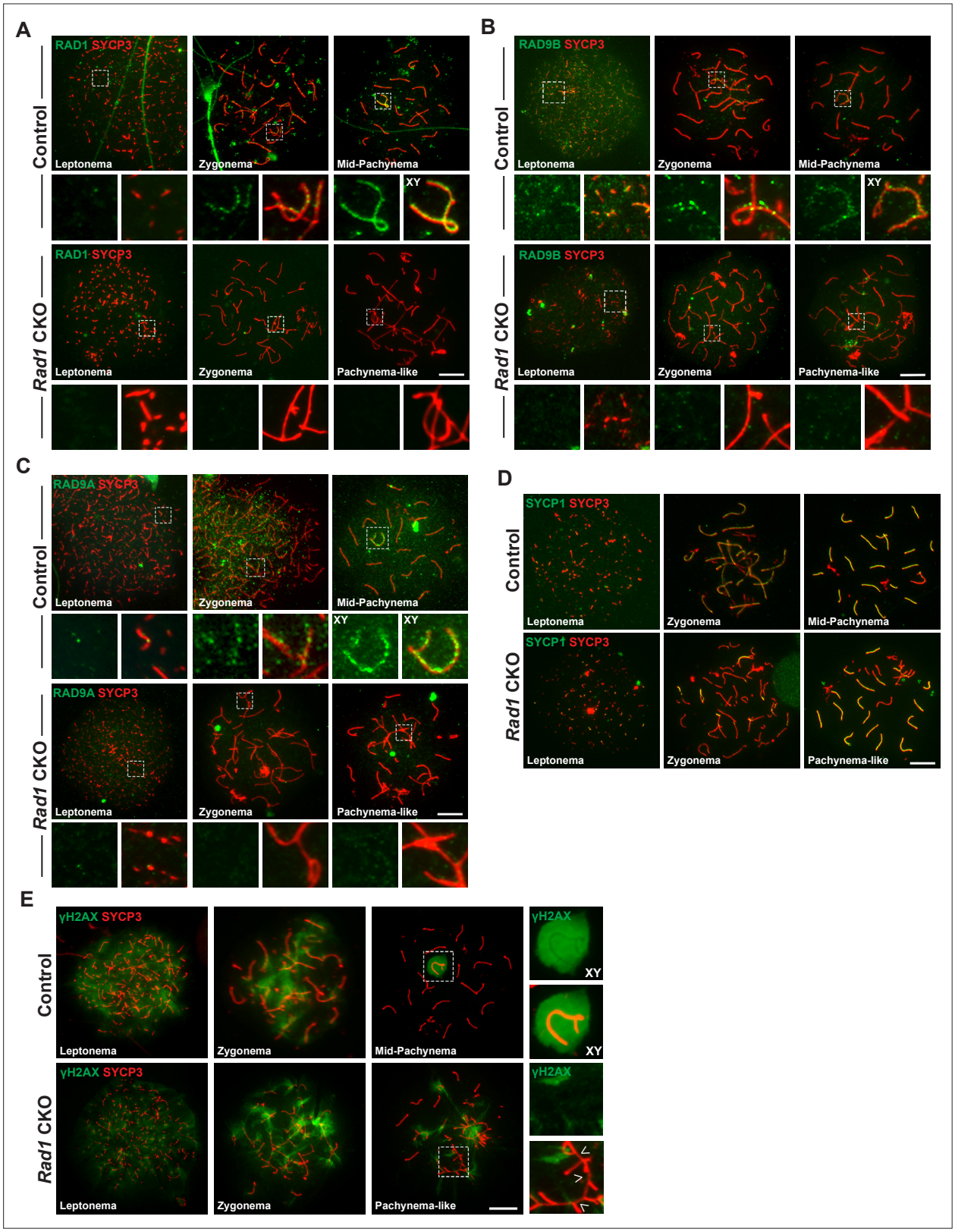

Figure 3. Testis-specific RAD1 loss disrupts 9-1-1 complex localization and causes defects in homolog synapsis and DNA damage signaling. (**A-C**) Meiotic spreads from 12-week-old control and *Rad1* conditional knockout (CKO) mice stained for RAD1 (**A**), RAD9B (**B**), or RAD9A (**C**). (**D**) Co-staining for SYCP1 and SYCP3 in meiotic spreads from 12-week-old control and *Rad1* CKO mice (three control mice, n = 156 cells; three CKO mice, n = 131 cells). *Rad1* CKO meiocytes with four or more synapsed chromosomes were categorized as pachytene-like. (**E**) γH2AX staining of meiotic spreads from control

Figure 3 continued on next page

Figure 3 continued

and *Rad1* CKO mice. Arrowheads in *Rad1* CKO spreads highlight regions of asynapsis lacking γH2AX staining (three control mice, n = 127 cells; five CKO mice, n = 205 cells). p-Values were calculated using Welch's unpaired *t*-test using GraphPad. Scale bar for A-E 10μm.

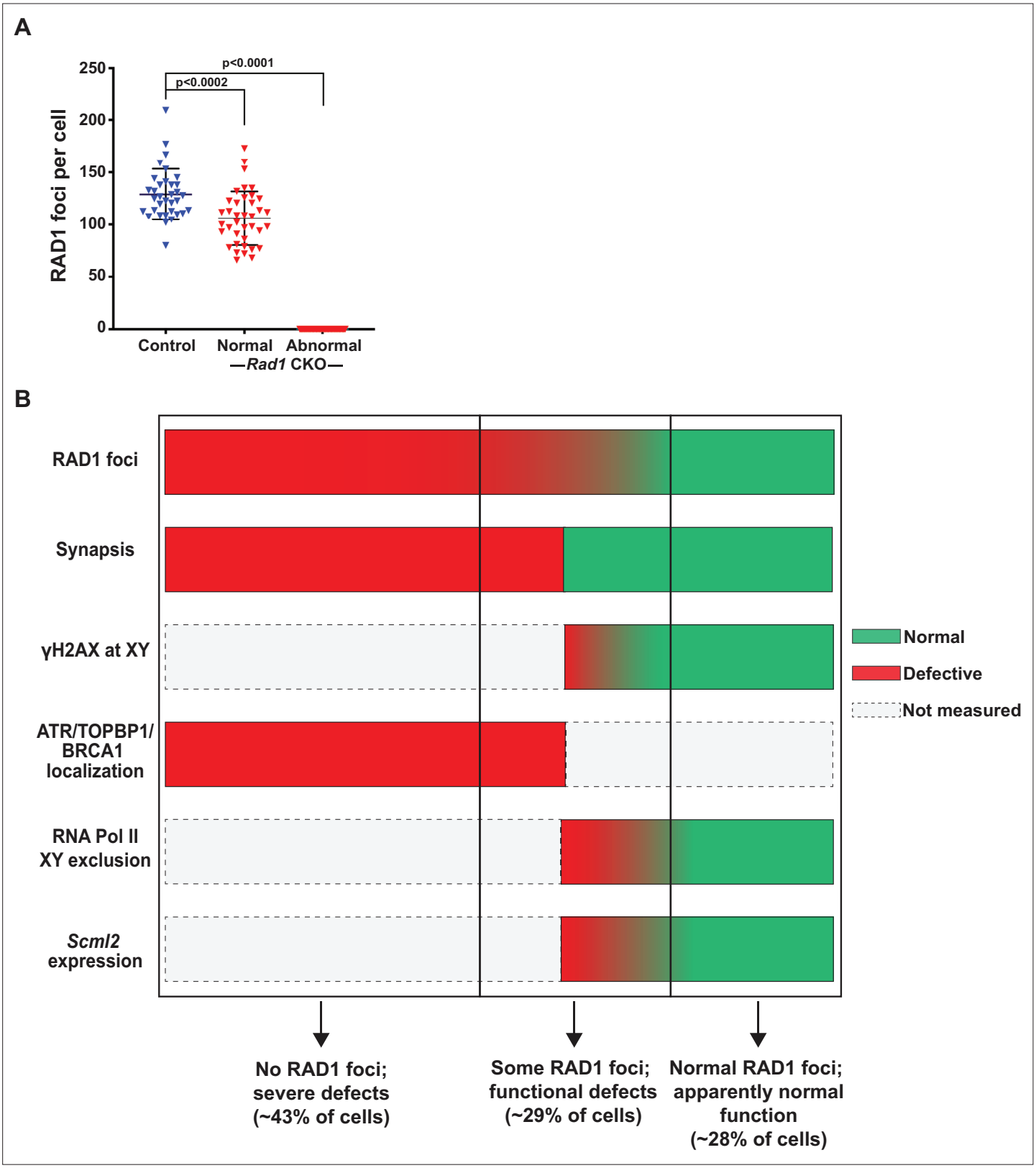

Figure 3—figure supplement 1. *Rad1* conditional knockout (CKO) spermatocytes vary in the extent of RAD1 loss and meiotic defects. (**A**) Total RAD1 foci counts in mid-pachytene control and *Rad1* CKO cells. Approximately equal numbers of *Rad1* CKO cells with apparently normal homolog synapsis (normal) or with synapsis defects (abnormal) were quantified (three control mice, n = 34 cells; three CKO mice, n = 38 normal and n = 40 abnormal cells). p-Values were calculated using Welch's unpaired *t*-test in GraphPad. (**B**) Summary image depicting three distinct RAD1 cell populations that

Figure 3—figure supplement 1 continued on next page

Figure 3—figure supplement 1 continued

are observed in *Rad1* CKO mice, based on RAD1 staining of meiotic chromosome spreads as well as the indicated functional assays. Cells in the first category (approximately 43% of CKO cells) lack RAD1 focus formation and have synapsis defects. Cells in the second category (approximately 29% of CKO cells) have detectable RAD1 focus formation but show at least one functional defect, including asynapsis or defects in meiotic sex chromosome inactivation. Cells in the third category (approximately 28% of CKO cells) display RAD1 focus formation and no apparent functional defects. See text for a detailed description of phenotyping and quantitation.

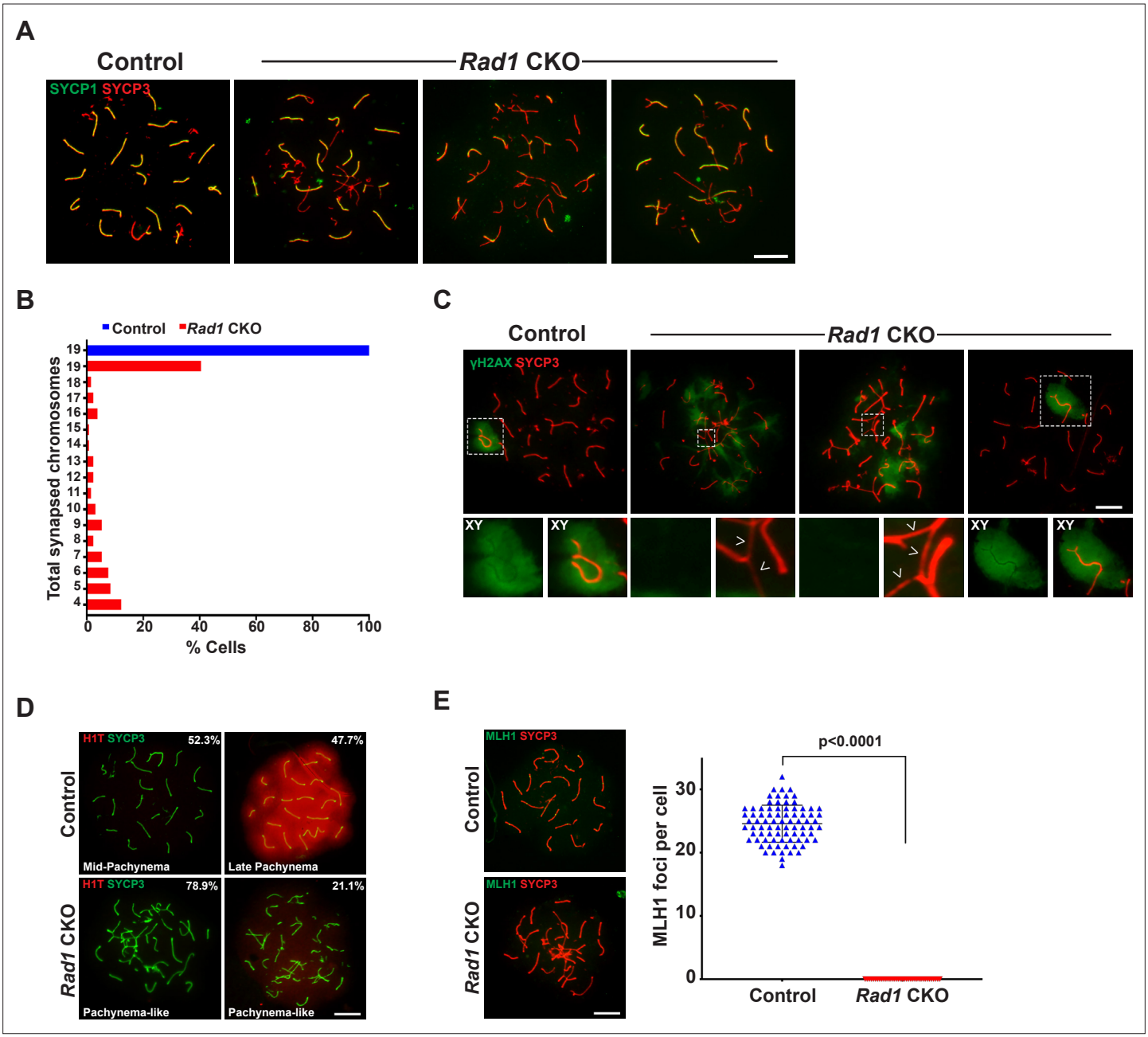

Figure 3—figure supplement 2. RAD1-deficient spermatocytes have synapsis defects and do not progress to mid-pachynema. (**A**) Examples of SYCP1/3 co-staining in control and *Rad1* conditional knockout (CKO) meiotic spreads (three control mice; n = 156 cells; three CKO mice; n = 131 cells). (**B**) Total synapsed chromosomes per cell in control (blue) and *Rad1* CKO (red) spermatocytes (three control mice, n = 156 cells; three CKO mice, n = 131 cells). (**C**) Additional examples of γH2AX meiotic spread staining in cells from control and *Rad1* CKO mice (three control mice, n = 127 cells; five CKO mice, n = 205 cells). Arrowheads in *Rad1* CKO spreads highlight regions of asynapsis lacking γH2AX staining. (**D**) H1T meiotic spread staining in cells from control and *Rad1* CKO mice. Of 174 pachynema staged cells analyzed from control mice, 52.3% of cells showed no H1T staining (two control mice, n = 258 cells). Of 104 pachynema-like staged cells from *Rad1* CKO mice, 78.9% of cells displayed no H1T and 21.1% showed low levels of H1T staining (two *Rad1* CKO mice, n = 104 cells). (**E**) Representative images of MLH1 staining in control and *Rad1* CKO spreads, and quantification of MLH1 foci (two control mice, n = 81 cells; two *Rad1* CKO mice, n = 37 cells). p-Values were calculated using Welch's unpaired *t*-test in GraphPad. Scale bars for A and C-E 10μM.

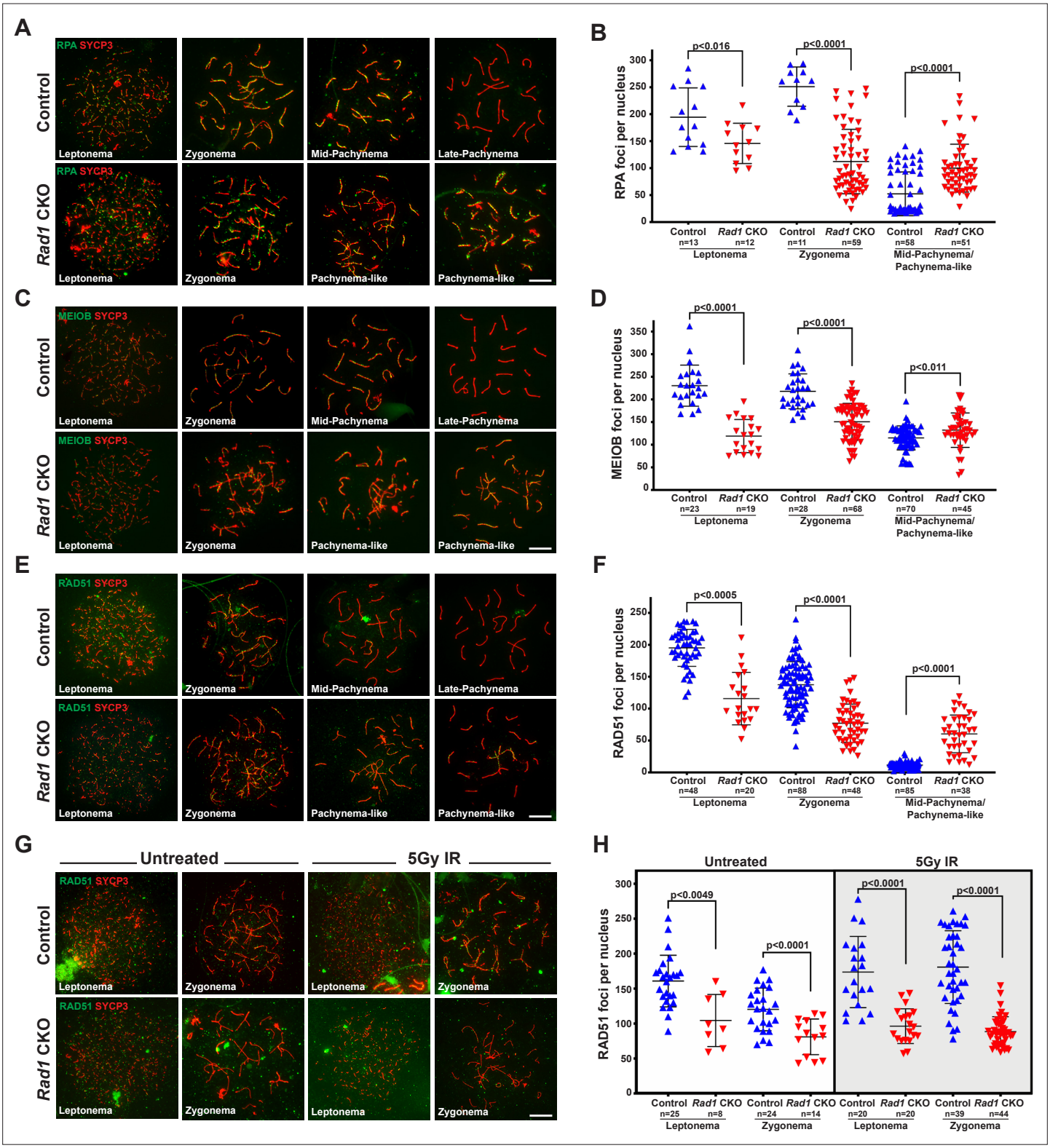

Figure 4. Double-strand break (DSB) repair is compromised in the absence of 9-1-1 complexes. (**A, B**) Representative images (**A**) and quantification (**B**) of RPA2 staining of meiotic spreads from 12-week-old control and *Rad1* conditional knockout (CKO) mice (three mice per genotype analyzed; n = total cells analyzed). (**C, D**) Representative meiotic spread images for ssDNA marker MEIOB (**C**) and quantifications (**D**) from 12-week-old control and *Rad1* CKO mice (three mice per genotype analyzed; n = total cells analyzed). (**E, F**) Representative meiotic spread images of RAD51 (**E**) and quantifications (**F**) from 12-week-old control and *Rad1* CKO mice (five control and six CKO mice; n = total cells analyzed). (**G, H**) 8-week-old control

Figure 4 continued on next page

Figure 4 continued

and *Rad1* CKO mice were irradiated with 5 Gy ionizing radiation (IR) and collected 1 hr post IR. Representative RAD51 meiotic spread images (**G**) and quantifications (**H**) (two control and two CKO mice; n = total cells analyzed). p-Values were calculated using Welch's unpaired *t*-test in GraphPad. Scale bars for A, C, E and G 10μm.

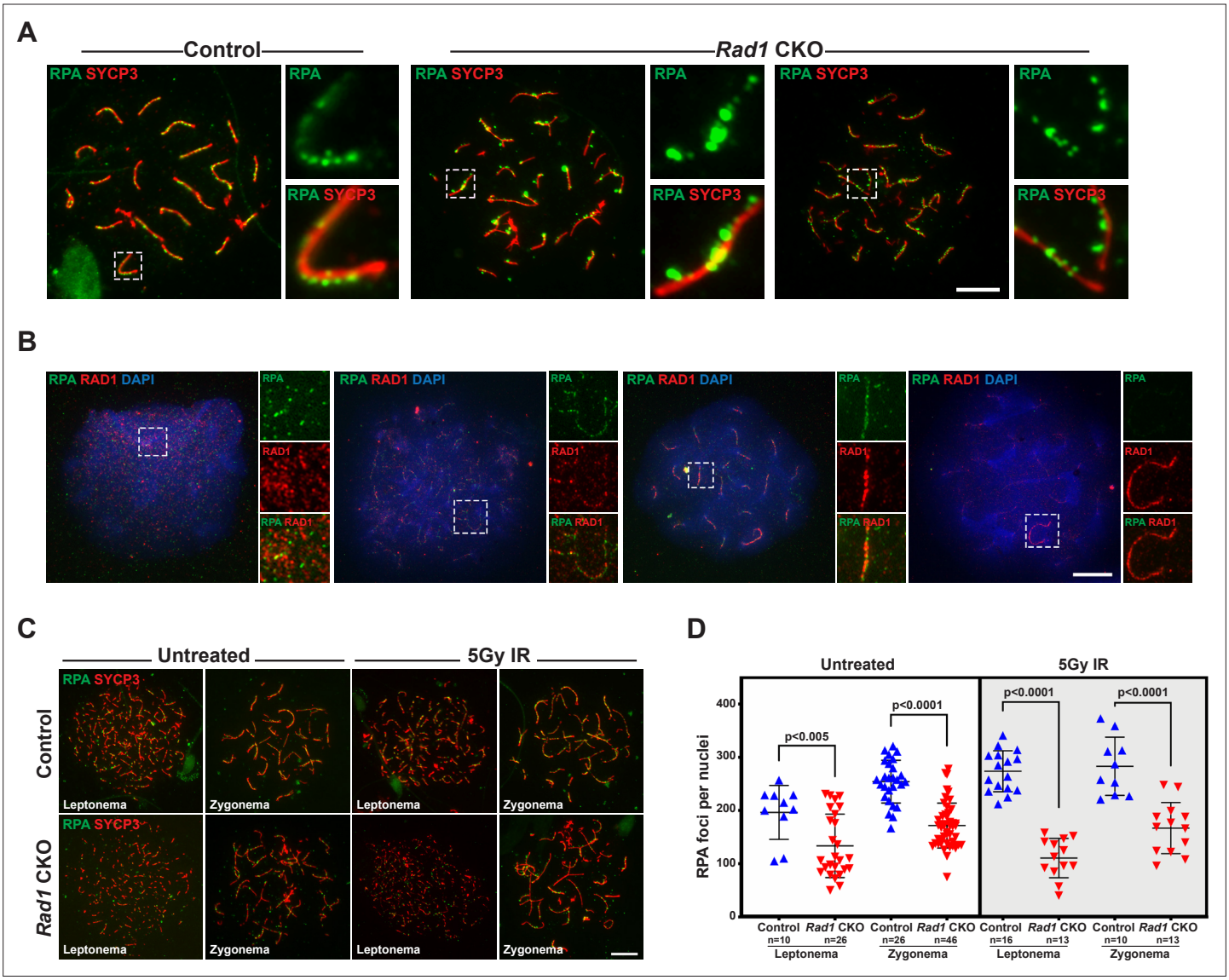

Figure 4—figure supplement 1. The 9-1-1 complexes are critical for proper localization of meiotic double-strand break (DSB) repair proteins. (**A**) Representative images of wild-type spermatocytes co-stained for RAD1 and RPA2 (three mice analyzed, n = 107 cells). (**B**) Representative images of control and *Rad1* conditional knockout (CKO) spermatocytes stained for RPA2 and SYCP3. Insers highlight the size of RPA2 foci observed in *Rad1* CKO spreads (three mice analyzed per genotype; n = 82 control cells; n = 122 CKO cells). (**C, D**) 8-week-old control and *Rad1* CKO mice were irradiated with 5 Gy ionizing radiation (IR and collected 1 hr post IR). Representative images (**C**) and quantification (**D**) of RPA2 staining of meiotic spreads prepared from mice of the indicated genotypes (two control and two *Rad1* CKO mice analyzed; n = total cells analyzed). p-Value calculated using Welch's unpaired *t*-test in GraphPad. Scale bars for A-C 10μm.

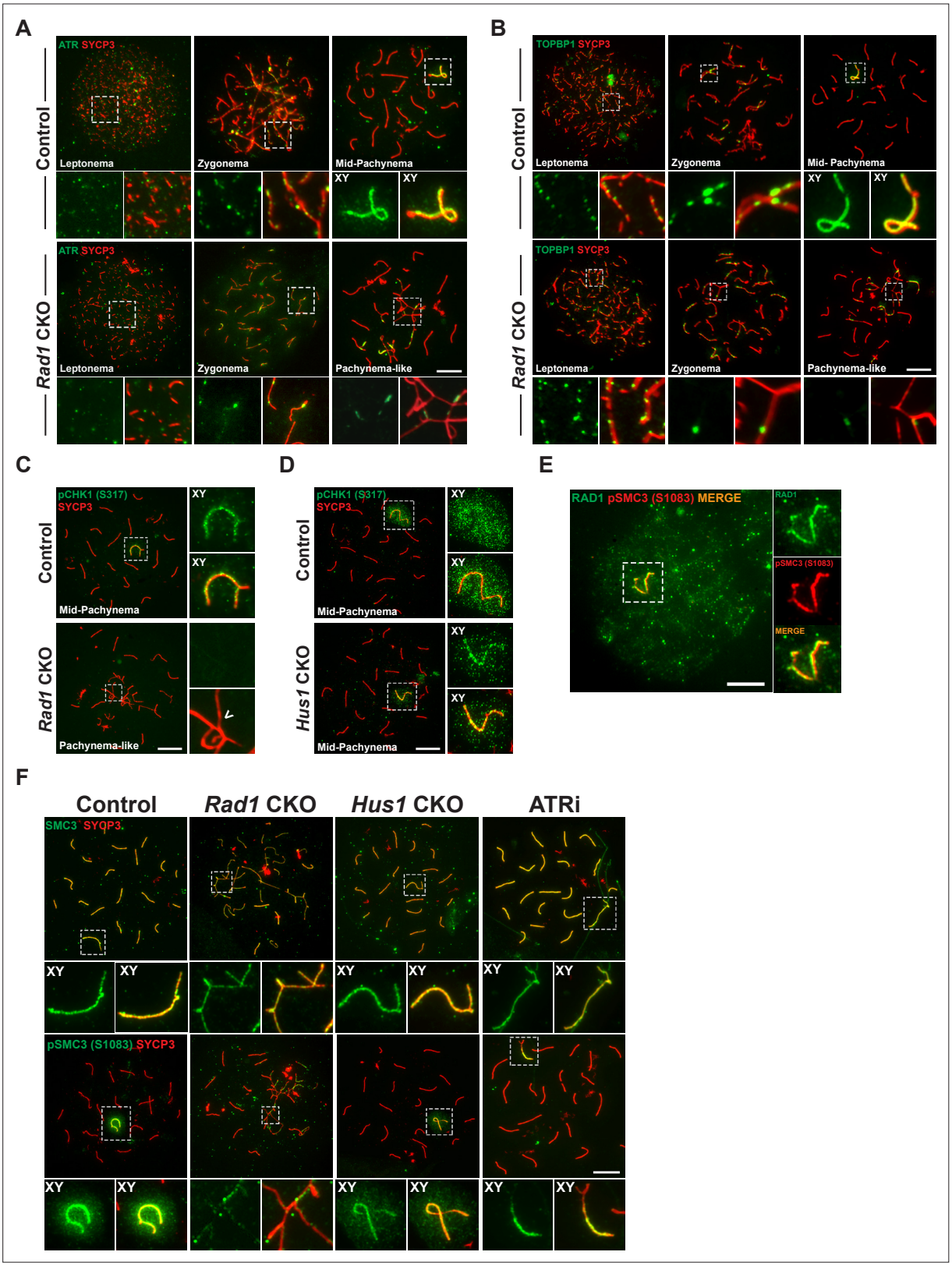

Figure 5. Key ATR phosphorylation events for double-strand break (DSB) repair and cohesion are dependent upon 9-1-1 complexes. (**A**) ATR localization in meiotic spreads from control and *Rad1* conditional knockout (CKO) 12-week-old mice (three control mice, n = 171 cells; three CKO mice, n = 146). (**B**) Representative images of TOPBP1 localization in meiotic spreads from 12-week-old control and *Rad1* CKO mice (three control mice, n = 130 cells; three CKO mice, n = 129). (**C, D**) Representative images of phospho-CHK1 (S317) localization in *Rad1* CKO (**C**) and *Hus1* CKO mice (**D**) (*Rad1* CKO:

Figure 5 continued on next page

Figure 5 continued

three control mice, n = 125 cells; three CKO mice, n = 120 cells; *Hus1* CKO: two control mice, n = 107 cells; three CKO mice, n = 191 cells). Arrowhead indicates a region of asynapsis. (**E**) Co-staining of RAD1 and pSMC3 (S1083) in wild-type spermatocytes. (**F**) Representative images of SMC3 and pSMC3 (S1083) localization in pachytene and pachytene-like cells from control, *Rad1* CKO, *Hus1* CKO, and ATRi-treated mice. Scale bars 10μm.

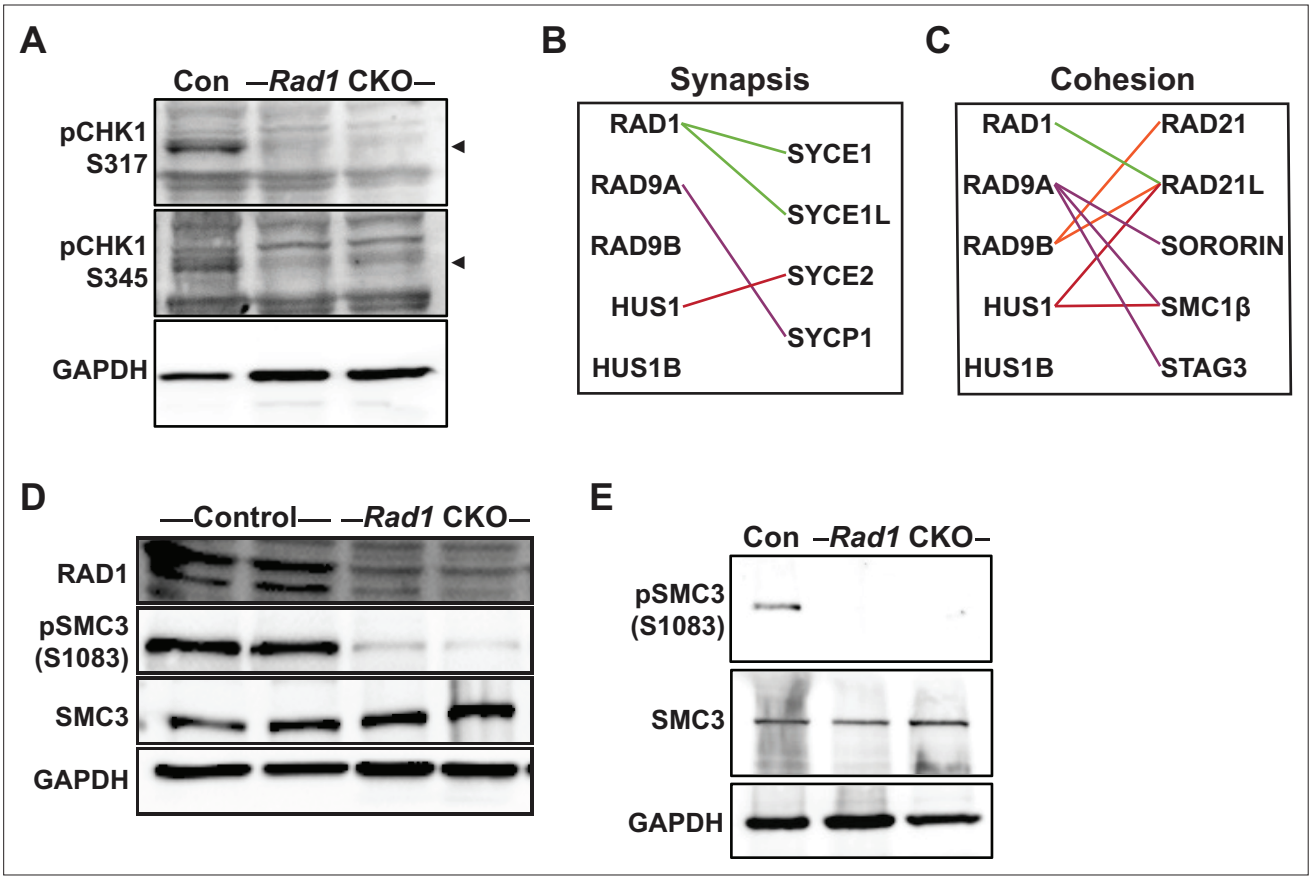

Figure 5—figure supplement 1. Phosphorylation of CHK1 and SMC3 is reduced in the absence of 9-1-1 complexes. (**A**) Representative immunoblots for phosphorylated pCHK1 (S317 and S345) in whole testis lysates from 8-week-old control and *Rad1* conditional knockout (CKO) mice. Arrowheads denote the pCHK1 band. (**B, C**) Evolutionary rate covariation (ERC) analysis between 9-1-1 complex subunits and synaptonemal complex (**B**) and cohesin (**C**) factors. Lines depict significant correlations observed between 9-1-1 complex subunits and synapsis or cohesin factors. (**D**) Representative immunoblot for phosphorylated SMC3 (S1083) and total SMC3 in whole testis lysates from 12-week-old control and *Rad1* CKO mice. (**E**) Representative immunoblot for pSMC3 (S1083) and SMC3 in whole testis lysates from 14-day-old control and *Rad1* CKO mice.

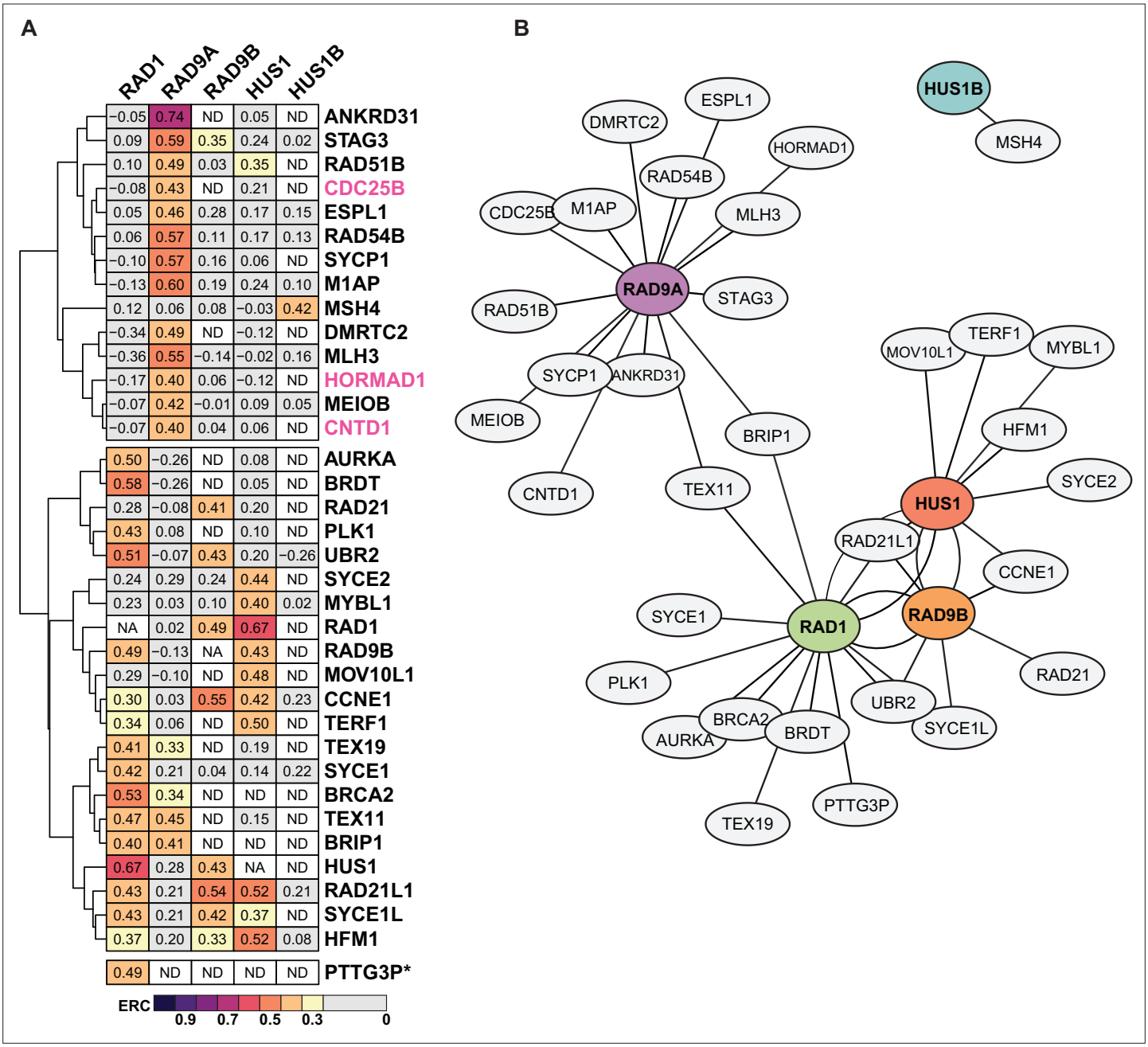

Figure 5—figure supplement 2. Evolutionary rate covariation (ERC) network of meiosis I proteins. (**A**) Heatmap of proteins found under Gene Ontology term meiosis I (GO:0007127) that showed ERC values ≥ 0.4 for each subunit. Pink labeling denotes proteins with no significant ERC values ($p>0.05$). ND: no value exists in dataset for paired comparison between the two proteins. NA: not applicable for comparisons between the same protein. PTTG3P* has a high ERC and significance with RAD1 only. (**B**) ERC values between subunits and meiosis I proteins were used to plot the network with force-directed layout. The Fruchterman and Reingold algorithm features attraction between highly connected nodes, identifying protein clusters based on ERC data. The distance between nodes is proportional to absolute edge weight (ERC value of each protein), with shorter distances between nodes reflecting higher ERC values.

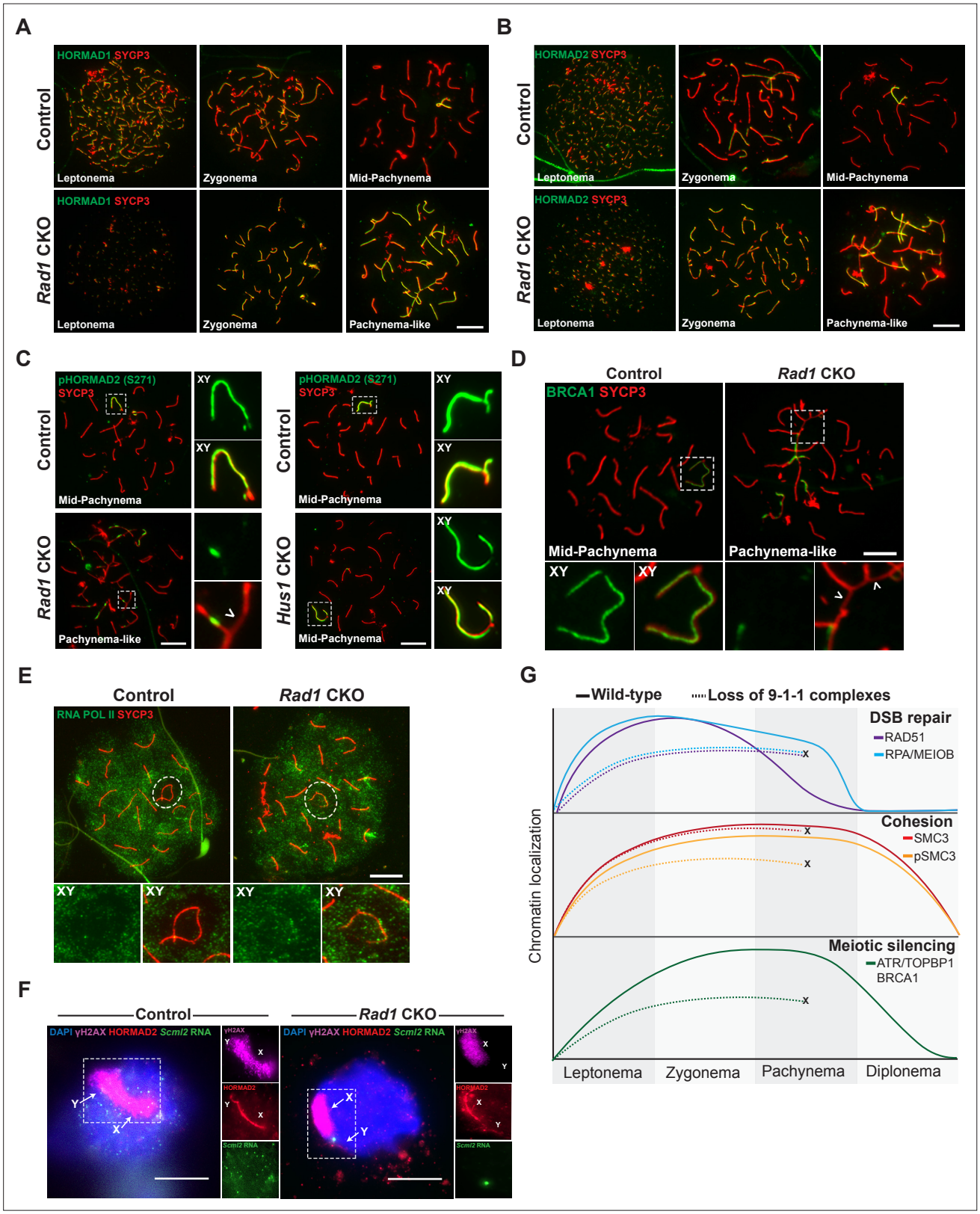

Figure 6. 9-1-1 complexes are required for ATR-mediated meiotic sex chromosome inactivation. (**A, B**) Representative images of HORMAD1 (**A**) and HORMAD2 (**B**) localization in meiotic spreads from 12-week-old control and *Rad1* conditional knockout (CKO) mice (three control mice, n = 146 cells; three CKO mice, n = 119 cells). (**C**) Representative images of phospho-HORMAD2 (S271) localization in meiotic spreads from 12-week-old control and *Rad1* CKO mice (*Rad1* CKO: three control mice, n = 178 cells; three CKO mice, n = 146 cells; *Hus1* CKO: two control mice, n = 189 cells; three CKO

Figure 6 continued on next page

Figure 6 continued

mice, n = 145 cells). Arrowhead indicates a region of asynapsis. (**D**) Representative images of BRCA1 localization in meiotic spreads from 12-week-old control and *Rad1* CKO mice (two control, n = 110 cells; two CKO, n = 149 cells). Arrowheads indicate regions of asynapsis. (**E**) Representative images of RNA Pol II staining in meiotic spreads from 12-week-old control and *Rad1* CKO mice (three control, n = 125 cells; three CKO, n = 98 cells). Note that the *Rad1* CKO cell has apparently normal synapsis but incomplete exclusion of RNA Pol II from the sex body. (**F**) RNA fluorescent in situ hybridization for *Scml2* in fully synapsed, pachytene-stage control and *Rad1* CKO cells, with co-staining for γH2AX and HORMAD2 (three control mice, n = 29 cells; three CKO mice, n = 45 cells). (**G**) Summary graphic depicting the localization of key meiotic factors in wild-type versus *Rad1* CKO spermatocytes. Loss of 9-1-1 complexes resulted in failure to progress to late pachytene, as depicted by the 'X.' Double-strand break (DSB) repair markers, such as RAD51, were reduced in the absence of the 9-1-1 complexes. The cohesin subunit SMC3 localized properly in the absence of 9-1-1 subunits, but its phosphorylation was impaired in *Rad1* CKO spermatocytes. Meiotic silencing factors such as ATR, TOPBP1, and BRCA1 also failed to localize properly in the absence of the 9-1-1 complexes. Scale bars for A-F 10μm.